

Designing rotational motion of charges on plasmonic nanostructures excited by circularly polarized light

Naoki Ichiji*,¹ Takuya Ishida,¹ Ikki Morichika,¹ Daigo Oue,^{2,3} Tetsu Tatsuma,¹ and Satoshi Ashihara¹

¹*Institute of Industrial Science, The University of Tokyo,
4-6-1 Komaba, Meguro-Ku, Tokyo 153-8505, Japan**

²*Instituto de Telecomunicações, Instituto Superior Técnico, University of Lisbon, 1049-001 Lisbon, Portugal*

³*The Blackett Laboratory, Imperial College London, London SW7 2AZ, United Kingdom*

Rotational motion of charges in plasmonic nanostructures plays an important role in transferring angular momentum between light and matter on the nanometer scale. Although sophisticated control of rotational charge motion has been achieved using spatially structured light, its extension to simultaneous excitation of the same charge motion in multiple nanostructures is not straightforward. In this study, we perform model calculations to show that spatially homogeneous circularly polarized (CP) light can excite rotational charge motions with a high degrees of freedom by exploiting the rotational symmetry of the plasmonic structure and that of the plasmon mode. Finite-difference time-domain simulations demonstrate selective excitation of rotational charge motion for both isolated nanoplates and periodic array structures, showing that complex charge rotations can be manipulated by plane CP waves in a wide range of plasmonic structures.

I. INTRODUCTION

The angular momentum transfer between light and matter has been extensively studied for more than a century. Various attempts have been made to transfer the angular momentum of light, including the spin angular momentum (SAM) or orbital angular momentum (OAM), to materials [1, 2]. These attempts include the induction of spinning and orbital motions of nanoparticles [3–7], fabrication of chiral nanostructures [8–11], and mass transfer in polymers [12, 13]. Angular momentum transfer also causes various interesting phenomena related to the angular momentum of light, such as circularly polarized light scattering [14], higher harmonic generation with handedness inversion [15], and enhancement of inverse Faraday effect [16–18].

Recently, several studies demonstrated that structured light with a designed spatial phase distribution can directly transfer their angular momentum to the rotational charge motion in plasmonic structures [19–22]. For example, a vortex beam with $-2\hbar$ OAM and $-\hbar$ SAM can transfer a total of $-3\hbar$ angular momentum to plasmonic structure. This results in their charges rotating by $2\pi/3$ in one oscillation period (Figure 1 (a)).

Although direct transfer of angular momentum by structured light enables the control of charge motion with a high degree of freedom, this transfer typically occurs around the phase singularity—where the intensity is minimal. This limitation restricts both the excitation efficiency of the induced charge motion and the number of objects that can be excited. To simultaneously and uniformly excite the same rotational motion in numerous structures—ideal for observing and manipulating physical phenomena such as induced magnetic fields [18, 23], the rotational Doppler effect [24], and evanescent fields

with SAM [25]—excitation with spatially homogeneous light is desirable.

Spatially homogeneous, circularly polarized (CP) light may have great potential for simultaneously exciting rotational motion in numerous structures [16]. An inherent limitation of homogeneous CP light in controlling rotational charge motion is that the angular momentum of the CP light can attain one of only two states: right or left-handed. Usually, the rotational charge motion induced by the CP light intuitively follows the rotation of the electric field, either right- or left-handed, which renders the altering of the direction or speed of the rotational motion challenging (Figure 1 (b)). However, a numerical calculation on the torque acting on plasmonic structures induced by CP light has showed an intriguing phenomenon: charges on a plasmonic nanoplate excited by plane CP light rotate in different directions, depending on the rotational symmetry of the plate and the order of plasmonic resonance [26]. The fact that the motion of charges excited by CP waves deviates from the rotation of the incident electric field suggests that the rotational charge motion can be manipulated with a high degree

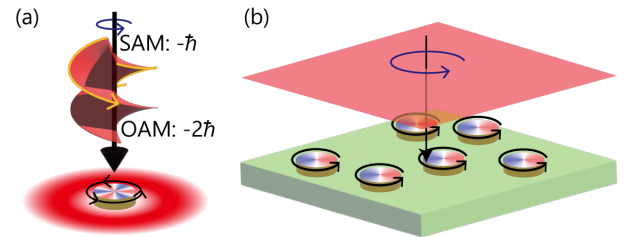


FIG. 1: Schematics of the rotational motion of the charge density on the plasmonic structures excited by (a) vortex beam and (b) spatially homogeneous circularly polarized light. Black arrows indicate the charge rotation per oscillation period.

* ichiji@iis.u-tokyo.ac.jp

of freedom by a plane CP wave through the geometric design of the plasmonic structure.

For the advanced control of rotational charge motion using CP light, it is essential to accurately grasp how the geometry of the plasmonic structure affects charge motions. In this study, we performed model calculations to show how the rotational symmetry of the plasmonic structure and that of the plasmon mode affect the rotational charge motion. We found that the proper selection of these two rotational symmetries enables the selective excitation of complex rotational charge motions with homogeneous CP light. The analytically obtained insight in this study can be generally applicable to versatile systems that have rotational symmetry, including regular nanoplates. Finite-difference time-domain (FDTD) simulations validated the charge behavior predicted by the analytical model for both single nanoplates and periodically arranged hole structures. These results suggest that the rotational charge motion could be manipulated by plane CP light in a wide range of plasmonic structures.

II. MODEL CALCULATIONS ON AZIMUTHALLY PERIODIC SYSTEMS

A. C_4 symmetry

Model calculations were performed to predict the rotational motion of charges in plasmonic nanostructures with different rotational symmetries. First, we consider a plasmonic system with C_4 symmetry and its azimuthal periodic plasmon modes. The charge density for the azimuthal periodic plasmon mode excited by x -polarized linearly polarized (LP) light, $\rho_m^{x\text{pol}}(r, \theta)$, is expressed in polar coordinates using radius r and angle θ as follows.

$$\rho_m^{x\text{pol}}(r, \theta) = A(r) \cos[m\theta], \quad (1)$$

where $A(r)$ denotes the radial distribution. The variable m is a positive integer that represents the order of the rotational symmetry of the charge density, where $m = 1, 2$, and 3 correspond to the dipole, quadrupole, and hexapole modes, respectively [20].

In a system with C_4 symmetry, the charge density excited by y -polarized LP light, $\rho_m^{y\text{pol}}(r, \theta)$, is required to be exactly equal to $\rho_m^{x\text{pol}}$ rotated by $\pi/2$. This can be expressed as

$$\begin{aligned} \rho_m^{y\text{pol}}(r, \theta) &= \rho_m^{x\text{pol}}(r, \theta - \pi/2) \\ &= A(r) \cos[m(\theta - \pi/2)]. \end{aligned} \quad (2)$$

By classifying the odd-order resonance modes into $m = (4j \pm 1)$ using integer j , we can divide Eq. 2 as follows:

$$\rho_{m=4j\pm 1}^{y\text{pol}}(r, \theta) = \pm A(r) \sin[m\theta]. \quad (3)$$

Note that even-order modes are forbidden in C_4 symmetric systems. The modeled $\rho_m^{x\text{pol}}$ and $\rho_m^{y\text{pol}}$ for the dipole mode, $m=1=4 \cdot 0 + 1$ ($j=0$), and those of the hexapole

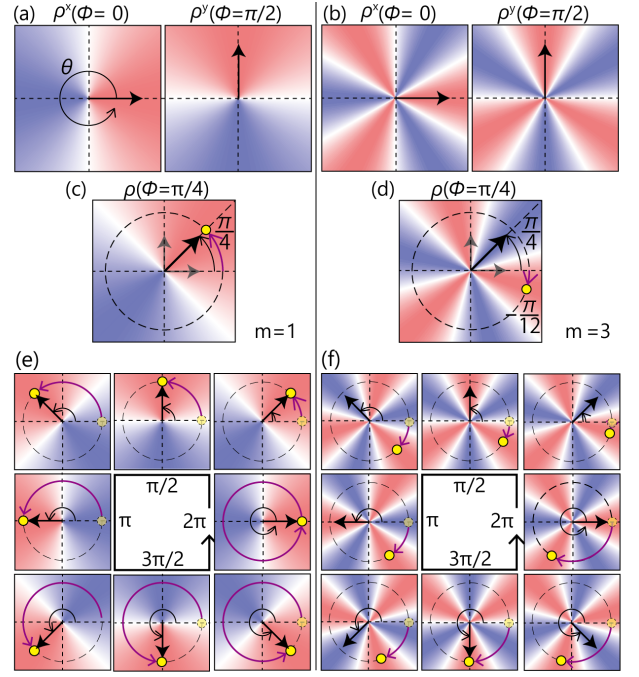


FIG. 2: (a,b) Simplified charge density distribution of the (a) dipole and (b) hexapole mode excited by x - and y -polarized linearly polarized (LP) light, respectively. The black arrows indicate the direction of the electric field of excitation light. (c and d) Charge distributions with $\phi = \pi/4$, calculated from the charge density of each of the x - and y -polarized excitation. The yellow circular markers and purple arrows indicate the angular shift where the charge density is maximum. (e and f) Angular distribution of charge density under circularly polarized excitation for one oscillation period.

mode, $m=3=4 \cdot 1 - 1$ ($j=1$), are plotted in Figures 2 (a) and (b), respectively. $A(r)$ is set to 1 for simplicity.

The charge density distribution excited by the LP light with a polarization angle ϕ , $\rho_m(r, \theta; \phi)$, is expressed as a superposition of the charge distribution excited by x -polarized light and that excited by y -polarized light,

$$\rho_m(r, \theta; \phi) = \rho_m^{x\text{pol}}(r, \theta) \cos[\phi] + \rho_m^{y\text{pol}}(r, \theta) \sin[\phi]. \quad (4)$$

From Eqs. 1-4, the charge density distribution of order $m=4j \pm 1$ can be transformed as follows.

$$\begin{aligned} \rho_{m=4j\pm 1}(r, \theta; \phi) &= A(r) (\cos[m\theta] \cos[\phi] \pm \sin[m\theta] \sin[\phi]) \\ &= A(r) \cos \left[m \left(\theta \mp \frac{\phi}{m} \right) \right] = \rho_m^{x\text{pol}} \left(r, \theta \mp \frac{\phi}{m} \right). \end{aligned} \quad (5)$$

Equation 5 indicates that the charge distribution $\rho_m(r, \theta; \phi)$ is equal to $\rho_m^{x\text{pol}}(r, \theta)$ rotated by ϕ/m counterclockwise (clockwise) for $m=4j+1$ ($m=4j-1$).

In Figures 2 (c) and (d), we plot the calculated charge density distribution excited by LP light with polarization

angle $\phi = \pi/4$, $\rho_1(\theta; \phi = \pi/4)$ and $\rho_3(\theta; \phi = \pi/4)$. In the dipole mode plotted in Figure 2 (c), the angle at which the charge density exhibits its maximum value is oriented $\pi/4$, aligning with the direction of the electric field. Conversely, in the hexapole mode, the maximum charge density shifts in the opposite direction to the shift of the electric field by $-\pi/12$.

It is noteworthy that the the charge density beneath the black arrow (aligned with the electric field vector) is positive for both horizontal and vertical polarizations (Figure 2 (b)), but turns negative for diagonal polarization (Figure 2 (d)). This non-intuitive charge distribution cannot occur in systems with C_8 symmetry, such as regular octagons and isotropic disks, where $\rho(\theta - \pi/4)$ must be $\rho(\theta)$ rotated clockwise by $\pi/4$. C_4 -symmetric systems lack C_8 symmetry, resulting in horizontal and diagonal excitations producing fundamentally distinct outcomes (i.e., $\rho(\theta - \pi/4)$ differs from $\rho(\theta)$ rotated clockwise by $\pi/4$).

Under CP light irradiation, ϕ continuously varies from 0 to $\pm 2\pi$ within an oscillation period. Figures 2 (e) and (f) show the time evolution of the angular charge density distribution for modes $m = 1$ and 3, over one oscillation period (ϕ varies continuously from 0 to 2π), corresponding to the incidence of left-handed CP light. For the dipole mode, the angle at which the charge density attains its maximum value, indicated by the yellow marker and purple arrow, follows the rotation of the electric field and rotates 2π per oscillation period. In contrast, the angle of maximum charge density in the hexapole mode rotates in the direction opposite to the rotation of the electric field, with a rotation angle of $2\pi/3$ per oscillation period.

B. C_N symmetric system

We now extend our discussion to general rotationally symmetric systems. The C_N rotationally symmetric systems require the following symmetry, using $\phi_N = 2\pi/N$,

$$\rho_m^N(r, \theta; \phi_N) = \rho_m^{x\text{pol}}(r, \theta - \phi_N) = A(r) \cos[m(\theta - \phi_N)], \quad (6)$$

where, $\rho_m^N(r, \theta; \phi_N)$ represents the charge density excited by the LP light with polarization angle ϕ_N . From Eq. 4, $\rho_m^{y\text{pol}}(r, \theta)$ can be expressed as

$$\begin{aligned} \rho_m^{y\text{pol}}(r, \theta) &= \frac{\rho_m^N(r, \theta; \phi_N) - \rho_m^{x\text{pol}}(r, \theta) \cos[\phi]}{\sin[\phi]} \\ &= A(r) \frac{\cos[m(\theta - \phi_N)] - \cos[m\theta] \cos[\phi]}{\sin[\phi]}. \end{aligned} \quad (7)$$

By substituting $m = (Nj \pm 1)$, the first term of the numerator in Eq. 7, $\cos[m(\theta - \phi_N)]$, can be transformed to

$$\cos[m(\theta - \phi_N)] = \cos[m\theta \mp \phi_N], \quad (8)$$

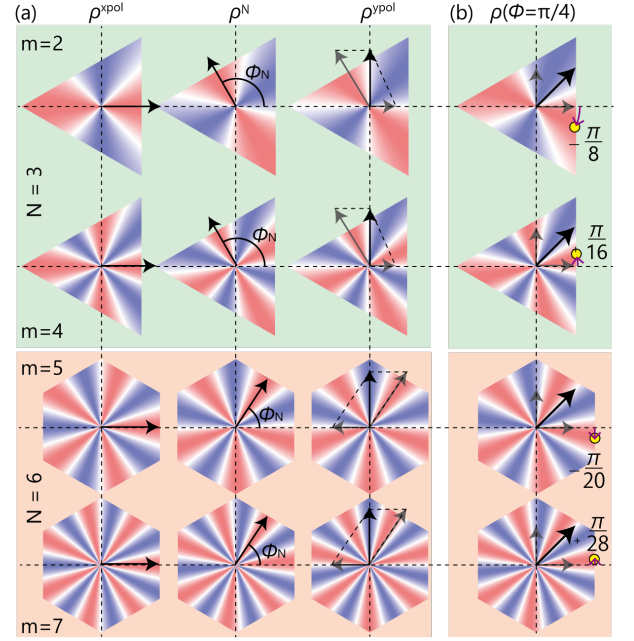


FIG. 3: (a) Calculated charge density distributions in the C_3 (top panel) and C_6 (bottom panel) symmetric system. From the left to right column, the polarization of the excitation lights is $\phi = 0$, $\phi = \phi_N = 2\pi/N$, and $\phi = \pi/2$. (b) Calculated charge density distributions for $\phi = \pi/4$. The yellow markers and purple arrows indicate the angular shift where the charge density is maximum.

because $Nj\phi_N = 2\pi j$. From Eqs. 7 and 8, following expression can be derived for the case $m = Nj \pm 1$, as in Eq. 3,

$$\rho_{m=Nj\pm 1}^{y\text{pol}}(r, \theta) = \pm A(r) \sin[m\theta]. \quad (9)$$

Here, $\rho_m^{x\text{pol}}$, ρ_m^N , and calculated $\rho_m^{y\text{pol}}$ for the case of $m = N \pm 1$ ($j = 1$) in the system with rotational symmetry of $N = 3$ ($m = 2, 4$) and $N = 6$ ($m = 5, 7$) are plotted in Figure 3 (a). Note that the triangular and hexagonal frames here, and the square frames in Figure 2, are introduced as typical representations of each rotational symmetry and do not indicate a specific geometry. Owing to Eqs. 3 and 9 being identical except for the N , the angular distribution of the m -th order mode excited by the LP light with angle ϕ for the C_N rotational symmetry can also be expressed as

$$\rho_{m=Nj\pm 1}(r, \theta; \phi) = \rho_m^{x\text{pol}}\left(r, \theta \mp \frac{\phi}{m}\right). \quad (10)$$

Considering the rotation of the electric field for CP light, Eq. 10 indicates that the rotational charge motion in a generalized rotational system can be described as follows: the charge density distribution of azimuthal periodic modes with $m = Nj \pm 1$ -order excited in C_N symmetric system rotates by $\pm 2\pi/m$ in one oscillation period.

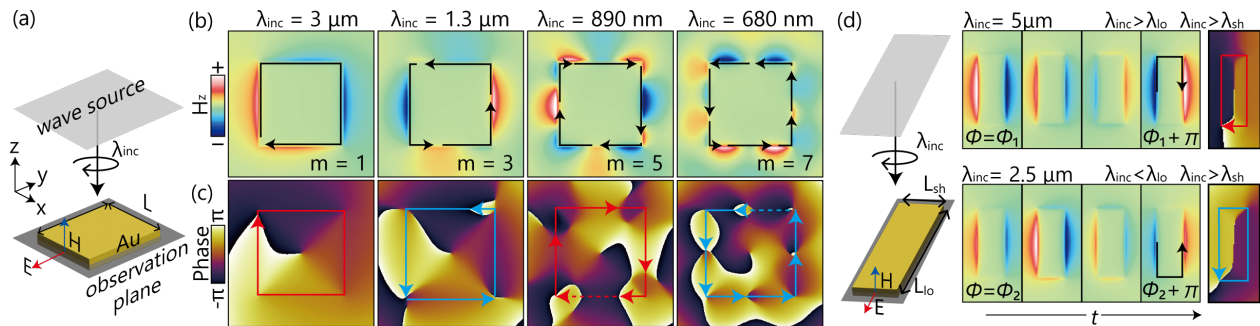


FIG. 4: (a) Schematic of the FDTD simulation model showing the setup with a wave source, an Au plate in the xy -plane, and an observation plane. (b) Spatial distributions of the H_z component at a representative phase for a square plate with $L=1 \mu\text{m}$, excited by circularly polarized (CP) light. (c) Spatial phase distributions of the H_z component plotted in (b). (d) Spatial distributions over half an oscillation period and spatial phase distributions of H_z components for a rectangular nanoantenna at $\lambda=5 \mu\text{m}$ (top panels) and $2.5 \mu\text{m}$ (bottom panels).

Calculated charge density distributions, $\rho_m(\theta; \phi = \pi/4)$ for the $m = N \pm 1$ -th modes, are plotted in Figure 3 (b). Similar to the C_4 system shown in Figure 2, the rotational direction of the charge density distribution for each mode is aligned with that of the electric field for $m = Nj + 1$ and opposite for $m = Nj - 1$. The amount of the rotation angle is ϕ/m in both cases.

It should be noted that the direction and speed of rotation of the charge density obtained here are consistent with one of the accessible OAM values of the far-field scattered field from a rotationally symmetric scatterer excited by CP light [26]. The relationship between the rotational symmetry of the scatterer and the possible OAM values of the far-field scattered field can be understood based on the concept of angular grating, which extends the linear grating to azimuthal periodic polar systems [15, 27–29]. Our calculations confirm the similarity between the rotational motion of charges within the plasmonic structure and far-field scattered field, both governed by the same restriction of rotational symmetry.

III. FDTD SIMULATION

A. Isolated nanoantenna

To confirm the validity of the model calculations, we evaluated the temporal evolution of the near-field electromagnetic distribution around plasmonic structures using FDTD simulations. Figure 4 (a) shows a schematic of the model used in the FDTD simulation. A 50 nm thick Au plate with side length $L=1 \mu\text{m}$ is placed in the xy -plane, and CP light with wavelength λ_{inc} is normally incident from a total-field scattered-field (TFSF) source located $5 \mu\text{m}$ away. The boundary conditions for the x , y , and z -directions are perfect matched layers (PML), and the minimum mesh width is 10 nm. The dielectric function of Au is obtained from the Palik database [30]. The observation plane is set in the middle of the Au layer to

record electric field \mathbf{E} and the magnetic field \mathbf{H} . All simulations were performed using ANSYS Lumerical (2023 R1). Since the plasmon waves with a fixed propagation direction have a magnetic field perpendicular to the propagation direction, the excited plasmon mode and their propagation directions can be evaluated from the spatial distribution of the magnetic field. Here, we evaluate the H_z distribution at the perimeter of the nanoplates to assess the plasmon mode orbiting the outer wall.

The spatial distributions of the H_z components at the characteristic wavelengths in the square nanoantenna are plotted in Figure 4 (b). From these distributions, we determined that the resonance orders m are 1, 3, 5, and 7 at wavelengths of $3 \mu\text{m}$, $1.3 \mu\text{m}$, $0.89 \mu\text{m}$, and $0.68 \mu\text{m}$, respectively. Trajectories of the positive H_z components during one oscillation period, evaluated from the time evolution of the magnetic field distribution for each wavelength, are plotted by black arrows in Figure 4 (b). Their direction and length indicate that the rotational directions at adjacent resonance orders are opposite each other, and that the amount of rotation per oscillation period is $2\pi/m$. These direction and speed of the rotation for each resonance mode are consistent with those obtained from Eq. 10.

Analogous to how the sign and magnitude of the OAMs of a vortex beam can be deduced from the spatial phase distribution of the electromagnetic field, the direction and speed of charge rotation on plasmonic structures can be evaluated from the spatial phase. Figure 4 (c) shows the spatial phase distribution of the H_z component for each wavelength plotted in Figure 4 (b). By examining the phase gradient along the perimeter of the square structure, both the direction of the phase gradient and the number of phase cycles per perimeter are observed to be dependent on the resonance order. The phase gradients from $-\pi$ to π along the perimeter are represented by red arrows for clockwise and blue arrows for counterclockwise. The direction of the phase gradient indicate that the rotational direction of the charges

in the $m=4j+1$ ($m=4j-1$) mode is the same (opposite) as that of the handedness of the excitation CP light. The region indicated by the dashed line, where the phase gradient is blurred and not distributed from $-\pi$ to π , is attributable to the contamination from off-resonant adjacent modes with peaks at close frequencies. In particular, at high frequencies, where the resonance frequencies are close to each other, the electromagnetic field distribution at each wavelength is affected by adjacent modes rotating in opposite directions.

In C_N systems where $N \geq 3$, m is uniquely represented by N and j , and thus the rotational direction is automatically determined from Eq. 10 for each resonance order. However, for a C_2 symmetric system, there are two ways to represent m , and the direction of charge rotation is not determined solely by rotational symmetry. For instance, the $m=1$ case in the C_2 symmetric system can be represented by $m=1=2 \cdot 0 + 1$ for $j=0$ and $m=1=2 \cdot 1 - 1$ for $j=1$; consequently, the charge density can rotate either to the clockwise or counter-clockwise. This is because $\rho_m^{y\text{pol}}$ is independent of $\rho_m^{x\text{pol}}$ in C_2 symmetric systems, unlike other rotationally symmetric systems with $N \geq 3$. Using Eq. 3, the charge density $\rho_m^{y\text{pol}}(r, \theta)$ for the y -polarized excitation in the above instance is estimated to be $+A(r) \sin \theta$ for $j=0$ and $-A(r) \sin \theta$ for $j=1$.

Such conditions can be designed by the geometry of the structure, or by the phase delay of the plasmonic charge motion owing to the difference between the resonance wavelength and the external field. In the optical resonance of rectangular nanoantennas, the long and short axes, having different resonance wavelengths, λ_{lo} and λ_{sh} , exhibit distinct phase delays relative to the external field [31]. When the external field wavelength (λ_{inc}) is much longer than both λ_{lo} and λ_{sh} , the resonances on both axes are in phase with the external field. Conversely, if λ_{inc} lies between λ_{lo} and λ_{sh} , the resonances on the short axis oscillate in phase, whereas those on the long axis oscillate out of phase.

The H_z components of a rectangular nanoantenna excited by CP light are plotted in Figure 4 (d), over a half oscillation period. The initial phase (ϕ_1, ϕ_2) is defined where the positive H_z is localized on the left side of the rectangle at each wavelength. The trajectories of positive H_z components for the half oscillation period are plotted with black arrows in the fourth image. The lengths of the long and short axes of the rectangle are 1.2 and 0.4 μm , respectively, and the evaluated resonance wavelengths are $\lambda_{\text{lo}}=3.6 \mu\text{m}$ and $\lambda_{\text{sh}}=1.8 \mu\text{m}$. At $\lambda_{\text{inc}}=5 \mu\text{m}$, which is a longer wavelength than both λ_{lo} and λ_{sh} , the H_z distribution rotates clockwise along the perimeter of the rectangle, which is the same as the handedness of the CP light (top panels). In contrast, at $\lambda_{\text{inc}}=2.5 \mu\text{m}$, which is located between λ_{lo} and λ_{sh} , the direction is reversed and counterclockwise rotation is observed (bottom panels). The phase distribution of H_z shown in right panels of Figure 4 (d) clearly indicates phase gradients in opposite directions.

These results confirm that the rotational behavior of

charges in isolated plasmonic nanoantennas is determined by the rotational symmetries of the structure and the resonance mode, as calculated using Eq. 10. In particular, the results for the rectangular nanoantenna exhibit that the geometric design of the plasmonic structure allows for the selective excitation of rotational charge motion.

B. Periodic lattice

As the only requirement for Eq. 10 is rotational symmetry, the discussion of the rotational behavior of charge densities is applicable to systems other than isolated plates, as long as they are rotationally symmetric. Circular structures, which generally allow only dipole mode for normally incident plane wave excitation because of their infinite rotational symmetry [19, 32], can exhibit multipole modes when their symmetry is restricted by an array structure [33, 34]. In other words, the multipole modes excited in the periodically arranged structure arise from the external rotational symmetry introduced by the arrangement. Therefore, the multipole modes excited by CP light in these periodic structures should also exhibit rotational behavior determined by the rotational symmetries.

Here we introduced C_4 and C_3 symmetry by arranging circular apertures in square and hexagonal lattice arrays, respectively, as illustrated in Figure 5(a). As with the isolated plate, the resonance order and rotational direction of the excited plasmon mode can be evaluated from the H_z component on the inner wall surface. From the simulation model for the isolated plate used in the previous section, the boundary condition in the xy direction is changed to a periodic boundary, and the TFSF wave source is replaced with a plane wave source. The lattice structure comprises a 50 nm thick Au thin film in vacuum, featuring an array of holes with radius r and lattice constant d . The minimum mesh size is reduced to 5 nm to minimize the effect of unintended C_4 symmetry introduced by the Yee lattice in the FDTD simulation.

Figure 5 (b) shows the spatial distributions of the H_z components at representative phases for different resonance orders. The trajectories of the positive H_z components per oscillation cycle are also plotted by black arrows, as in Figure 4 (b). The spatial phase distributions of H_z components are plotted in Figures 5 (c), and the phase gradient along the inner wall of the circular aperture is indicated by red and blue arrows. The rotation angle indicated by each arrow is approximately $2\pi/m$ and is opposite to the incident CP light only when $m=Nj-1$. This observation is consistent with Eq. 10.

It is noteworthy that the $m=5$ mode corresponds to $N+1$ for $N=4$ and $2N-1$ for $N=3$, indicating that multipole modes of the same order rotate in opposite directions on square and hexagonal lattices. These calculations demonstrate that the rotational symmetry introduced externally by the periodic array allows us to manipulate the uniform rotational motion of charges in

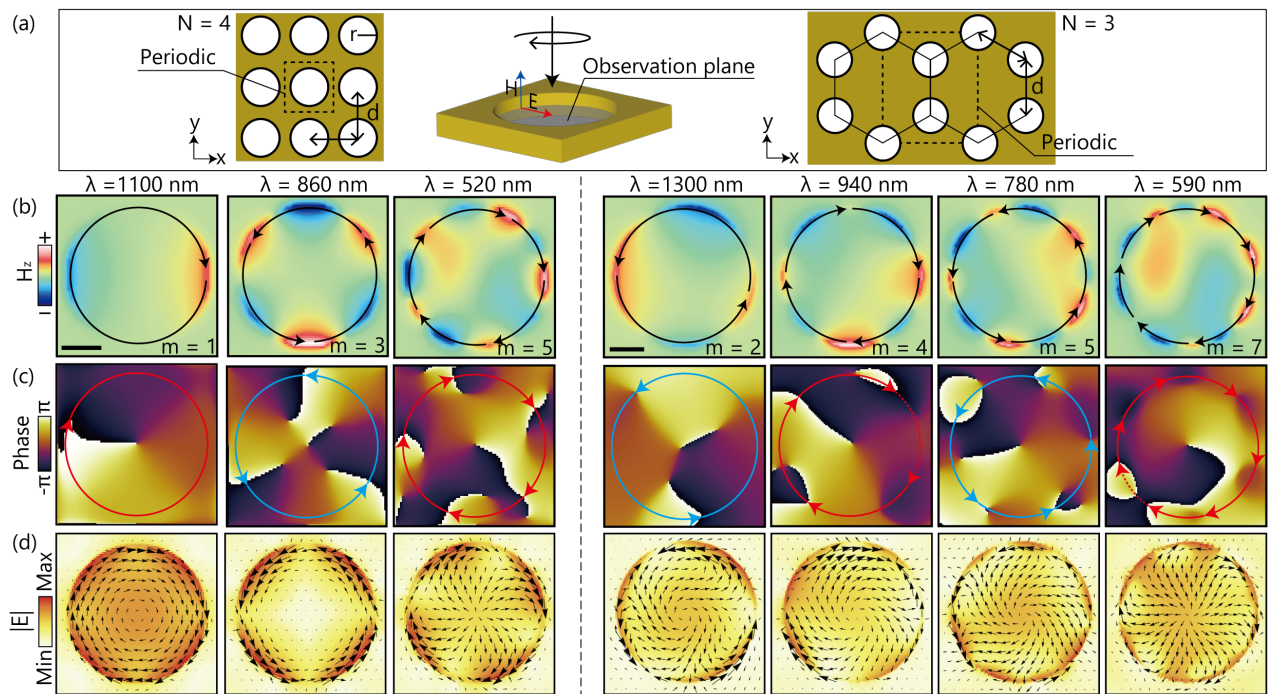


FIG. 5: (a) Schematic of the lattice structures used in the FDTD simulations. (b–d) Spatial distribution of the (b) H_z components at representative phase, (c) phase distributions of the H_z components, and (d) averaged intensity distributions of the electric field $|E|$ (color map) and Poynting vectors (black arrows). Calculations were performed with $r=350$ nm and $d=800$ nm for square lattices, and $r=400$ nm and $d=1200$ nm for hexagonal lattices. The scale bars in (b) represent 200 nm.

a wide range of plasmonic structures with a high degree of freedom using spatially homogeneous CP light.

One might think that the observed rotational motion of the charges could be due to shifts in the constructive interference position or the wagon wheel effect resulting from the discrete computation time. Here, we investigate the spatial distribution of the Poynting vector $\mathbf{P} = \text{Re}[\mathbf{E}^* \times \mathbf{H}]/2$, which represents the energy flow. Figure 5 (d) shows the in-plane components of the Poynting vectors, as black arrows on the color map of the averaged electric field intensity. The orientation of the Poynting vectors along the circumference corroborates that the clockwise and counterclockwise charge motions actually possess an energy flow consistent with their rotation direction. These energy flow indicate that the rotation of charges excited by CP light can be regarded as a surface current orbiting the plasmonic structure. The non-uniform intensity distribution and partially retrograde pointing vectors (e.g., the right side of $\lambda = 940$ nm for $N = 3$) are attributed to the contamination from off-resonant adjacent modes.

Manipulating the rotational motion of charge distributions in periodic plasmonic nanostructures shows that uniform control of rotational charge motion in large-area structures suitable for experimental observation is achievable. This capability offers a variety of potential applications, such as the observation of the inverse Fara-

day effect [16–18, 35, 36], designing the resonant interaction between magnetic resonance antennas [37], manipulation of the photocurrent [38–40] and spin currents [41–47], and control of the SAM associated with the plasmonic near-field [48–50].

The spatial phase distributions similar to those of vortex beams with higher-order OAMs observed in Figure 4 (c) and 5 (c) suggest the possibility of experimental investigations of light-matter interactions involving OAM [51–55]. Furthermore, our calculations indicate that the rotational charge motions on plasmonic structures excited by CP light exhibit opposite directions between adjacent modes among the multipole resonance modes that can be excited in each structure. This is important for explaining certain complex spatial distributions and non-intuitive temporal variations of electromagnetic fields often observed in electromagnetic simulations using CP excitation light [56], and aids in the calculation of the optical properties of enhanced electromagnetic fields, such as SAM [48] and optical chirality [57].

Although we limited the structures in each calculation to one type for simplicity, more complex rotational behavior of the charges can be designed by combining different structures. For instance, charges can be rotated in opposite directions on the same plane by using structures of different sizes that share the same rotational symmetry (see appendix). Designing geometries other than regular

polygons, such as swastikas, would facilitate a more efficient excitation of specific rotational behaviors. The actual charge density distribution in nanopolygon plates often does not exhibit the perfect azimuthal periodicity as simplified in this study [58, 59]. Defining basis vectors based on modal analysis that considers the geometry of each structure to evaluate such complex distributions is our future work [60].

IV. CONCLUSION

In conclusion, we numerically investigated the rotational charge behavior of nanoscale plasmonic structures excited by CP light. By simplifying the spatial distribution of the multipole plasmon modes, we formulated the manner in which the rotational symmetry of the plasmonic structure and that of the plasmon mode affect the charge motion. We showed that the direction and speed of charge rotation on the plasmonic structure could be controlled using spatially homogeneous CP light, by appropriately selecting these two rotational symmetries.

The FDTD simulations validated the charge behavior predicted by the analytical model for both single nanoplates and periodically arranged hole structures, thus demonstrating that the rotational charge motion could be effectively managed by plane CP light across a wide range of plasmonic structures. The findings on the rotational behavior of charges summarized in this study are expected to greatly aid in the experimental verification of light-matter interactions involving angular momentum.

ACKNOWLEDGMENTS

This work was supported by a Grant-in-Aid for JSPS Fellows (No.JP23KJ0355), a Grant-in-Aid for Scientific Research (A) (No. JP20H00325), and a Grant-in-Aid for Challenging Exploratory Research (No.JP20K20560). D.O. is supported by JSPS Overseas Research Fellowship, by the Institution of Engineering and Technology (IET), and by Fundação para a Ciência e a Tecnologia and Instituto de Telecomunicações under project UIDB/50008/2020.

Appendix A: Simulation results of combined structure

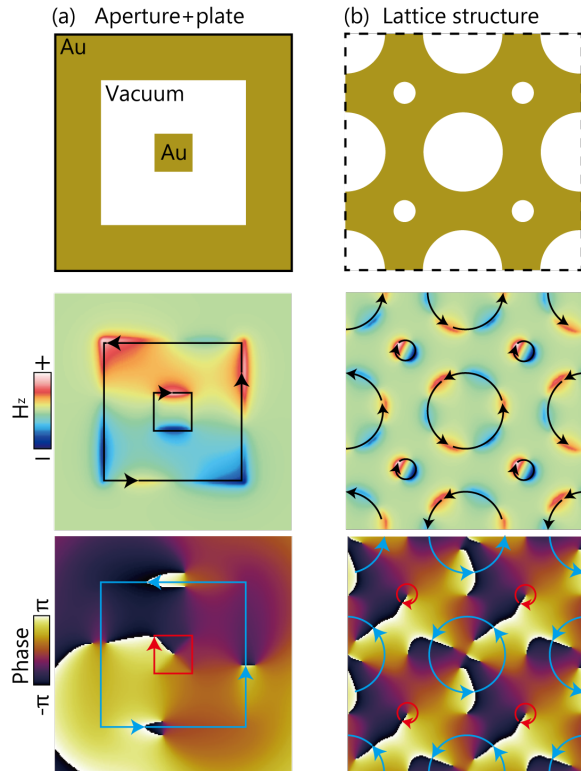


FIG. S1: Simulation results for plasmonic structures combining elements of different sizes sharing the same rotational symmetry, excited with circularly polarized light. (a) a combination of a large square aperture ($L = 600$ nm) with a small square plate ($L = 150$ nm) in the center. (b) a combination of C_4 symmetric lattice arrays of circular aperture structures with radii of 200 nm and 50 nm.

- [1] M. Friese, T. Nieminen, N. Heckenberg, and H. Rubinsztein-Dunlop, Optical alignment and spinning of laser-trapped microscopic particles, *Nature* **394**, 348 (1998).
- [2] A. B. Stilgoe, T. A. Nieminen, and H. Rubinsztein-Dunlop, Controlled transfer of transverse orbital angular momentum to optically trapped birefringent microparticles, *Nat. Photon.* **16**, 346 (2022).
- [3] Y. Zhao, D. Shapiro, D. Mcgloin, D. T. Chiu, and S. Marchesini, Direct observation of the transfer of or-

bitual angular momentum to metal particles from a focused circularly polarized gaussian beam, *Opt. Express* **17**, 23316 (2009).

- [4] F. Monteiro, S. Ghosh, E. C. van Assendelft, and D. C. Moore, Optical rotation of levitated spheres in high vacuum, *Phys. Rev. A* **97**, 051802 (2018).
- [5] H. Fujiwara, K. Sudo, Y. Sunaba, C. Pin, S. Ishida, and K. Sasaki, Spin-orbit angular-momentum transfer from a nanogap surface plasmon to a trapped nanodiamond, *Nano Lett.* **21**, 6268 (2021).

- [6] P. Karpinski, Rotation and revolution of optically trapped gold nanorods induced by the spin and orbital angular momentum of a laguerre-gaussian vortex beam, *Adv. Opt. Mat.* **10** (2022).
- [7] K. Wang, E. Schonbrun, P. Steinvurzel, and K. B. Crozier, Trapping and rotating nanoparticles using a plasmonic nano-tweezer with an integrated heat sink, *Nat. Commun.* **2** (2011).
- [8] K. Saito and T. Tatsuma, Chiral plasmonic nanostructures fabricated by circularly polarized light, *Nano Lett.* **18**, 3209 (2018).
- [9] K. Toyoda, F. Takahashi, S. Takizawa, Y. Tokizane, K. Miyamoto, R. Morita, and T. Omatsu, Transfer of light helicity to nanostructures, *Phys. Rev. Lett.* **110**, 143603 (2013).
- [10] K. Shimomura, Y. Nakane, T. Ishida, and T. Tatsuma, Photofabrication of chiral plasmonic nanospiroids, *Appl. Phys. Lett.* **122**, 151109 (2023).
- [11] T. Ishida, A. Isawa, S. Kuroki, Y. Kameoka, and T. Tatsuma, All-plasmonic-metal chiral nanostructures fabricated by circularly polarized light, *Appl. Phys. Lett.* **123**, 061111 (2023).
- [12] A. Ambrosio, L. Marrucci, F. Borbone, A. Roviello, and P. Maddalena, Light-induced spiral mass transport in azo-polymer films under vortex-beam illumination, *Nat. Commun.* **3**, 989 (2012).
- [13] A. Tomita, A. Valles, K. Miyamoto, and T. Omatsu, Creation of galaxy-shaped vortex relief structures in azopolymers with petal-like beams, *Opt. Express* **31**, 27868 (2023).
- [14] H. Negoro, H. Sugimoto, and M. Fujii, Helicity-preserving optical metafluids, *Nano Lett.* **23**, 5101 (2023).
- [15] K. Konishi, D. Akai, Y. Mita, M. Ishida, J. Yumoto, and K. Kuwata-Gonokami, Circularly polarized vacuum ultraviolet coherent light generation using a square lattice photonic crystal nanomembrane, *Optica* **7**, 855 (2020).
- [16] A. K. Gonzalez-Alcalde, X. Shi, V. H. Ortiz, J. Feng, R. B. Wilson, and L. T. Vuong, Enhanced inverse faraday effect and time-dependent thermo-transmission in gold nanodisks, *Nanophotonics* **13**, 1993–2002 (2024).
- [17] S. Parchenko, K. Hofhuis, A. A. Larsson, V. Kapaklis, V. Scagnoli, L. J. Heyderman, and A. Kleibert, Plasmon-enhanced optical control of magnetism at the nanoscale via the inverse faraday effect, *Adv. Photon. Res.* (2024).
- [18] O. H.-C. Cheng, D. H. Son, and M. Sheldon, Light-induced magnetism in plasmonic gold nanoparticles, *Nat. Photon.* **14**, 365–368 (2020).
- [19] K. Sakai, K. Nomura, T. Yamamoto, T. Omura, and K. Sasaki, Quadrupole lattice resonances in plasmonic crystal excited by cylindrical vector beams, *Sci. Rep.* **6** (2016).
- [20] T. Arikawa, T. Hiraoka, S. Morimoto, F. Blanchard, S. Tani, T. Tanaka, K. Sakai, H. Kitajima, K. Sasaki, and K. Tanaka, Transfer of orbital angular momentum of light to plasmonic excitations in metamaterials, *Sci. Adv.* **6**, eaay1977 (2020).
- [21] D.-J. Yang and J.-C. Liu, Selective high-order resonance in asymmetric plasmonic nanostructures stimulated by vortex beams, *Nanoscale* **15**, 11860 (2023).
- [22] D. Tanaka, S. Harajiri, Y. Fujita, K. A. Forbes, T. T. Pham, and D. L. Andrews, Multipole excitation of localized plasmon resonance in asymmetrically coated core-shell nanoparticles using optical vortices, *Laser & Photon. Rev.* **18**, 2300536 (2024).
- [23] O. H.-C. Cheng, B. Zhao, Z. Brawley, D. H. Son, and M. T. Sheldon, Active tuning of plasmon damping via light induced magnetism, *Nano Lett.* **22**, 5120–5126 (2022).
- [24] D. Pan, H. Xu, and F. J. García de Abajo, Circular dichroism in rotating particles, *Phys. Rev. Lett.* **123**, 066803 (2019).
- [25] K. Y. Bliokh, A. Y. Bekshaev, and F. Nori, Extraordinary momentum and spin in evanescent waves, *Nat. Commun.* **5**, 3300 (2014).
- [26] Y. E. Lee, K. H. Fung, D. Jin, and N. X. Fang, Optical torque from enhanced scattering by multipolar plasmonic resonance, *Nanophotonics* **3**, 343–350 (2014).
- [27] T. A. Nieminen, T. Asavei, V. L. Y. Loke, N. R. Heckenberg, and H. Rubinsztein-Dunlop, Symmetry and the generation and measurement of optical torque, *J. Quant. Spectrosc. Radiat. Transf.* **110**, 1472 (2009).
- [28] J. Parker, C. W. P. Etersson, Y. Yifat, S. A. Rice, Z. Yan, S. K. Gray, and N. F. Scherer, Optical matter machines: angular momentum conversion by collective modes in optically bound nanoparticle arrays, *Optica* **7**, 1341 (2020).
- [29] J. Chen, J. Ng, K. Ding, K. H. Fung, Z. Lin, and C. T. Chan, Negative optical torque, *Sci. Rep.* **4**, 6386 (2014).
- [30] E. D. Palik, *Handbook of Optical Constants of Solids* (Academic Press, 1985).
- [31] T. Oshikiri, Q. Sun, H. Yamada, S. Zu, K. Sasaki, and H. Misawa, Extrinsic chirality by interference between two plasmonic modes on an achiral rectangular nanostructure, *ACS Nano* **15**, 16802 (2021).
- [32] Y. Lan, Y. Xu, Y. Jia, T. Mei, S. Qu, B. Yan, D. Yang, B. Chen, R. Xu, and Y. Li, Multipole modes excitation of uncoupled dark plasmons resonators based on frequency selective surface at x-band frequency regime, *Sci. Rep.* **7** (2017).
- [33] Z. Yi, M. Liu, J. Luo, Y. Zhao, W. Zhang, Y. Yi, Y. Yi, T. Duan, C. Wang, and Y. Tang, Multiple surface plasmon resonances of square lattice nanohole arrays in Au-SiO₂-Au multilayer films, *Opt. Commun.* **390**, 1 (2017).
- [34] T. K. Hakala, H. T. Rekola, A. I. Vakevainen, J. P. Martikainen, M. Necada, A. J. Moilanen, and P. Torma, Lasing in dark and bright modes of a finite-sized plasmonic lattice, *Nat. Commun.* **8**, 13687 (2017).
- [35] V. Karakhanyan, C. Eustache, Y. Lefier, and T. Grosjean, Inverse faraday effect from the orbital angular momentum of light, *Phys. Rev. B* **105**, 045406 (2022).
- [36] Y. Mou, X. Yang, B. Gallas, and M. Mivelle, A reversed inverse faraday effect, *Adv. Mater. Technol.* **8**, 2300770 (2023).
- [37] N. Ichiji and A. Kubo, Resonance-order-dependent plasmon-induced transparency in orthogonally arranged nanocavities, *Opt. Lett.* **47**, 265 (2022).
- [38] W. Li, Z. J. Coppens, L. V. Besteiro, W. Wang, A. O. Govorov, and J. Valentine, Circularly polarized light detection with hot electrons in chiral plasmonic metamaterials, *Nat. Commun.* **6**, 8379 (2015).
- [39] L. Wang, J. Zheng, K. Wang, M. Khan, N. Hu, H. Li, L. Li, J. Wang, and W. Ni, Circular differential photocurrent mapping of hot electron response from individual plasmonic nanohelicoids, *ACS Appl. Mater. Interfaces* **16**, 24951 (2024).
- [40] Y. Mou, X. Yang, M. Vega, R. Zapata, B. Gallas, J.-F. Bryche, A. Bouhelier, and M. Mivelle, Femtosecond drift photocurrents generated by an inversely designed plas-

- monic antenna, *Nano Lett.* 10.1021/acs.nanolett.4c00558 (2024).
- [41] D. Oue and M. Matsuo, Effects of surface plasmons on spin currents in a thin film system, *New J. Phys.* **22**, 033040 (2020).
- [42] D. Oue and M. Matsuo, Electron spin transport driven by surface plasmon polaritons, *Phys. Rev. B* **101**, 161404(R) (2020).
- [43] D. Oue and M. Matsuo, Optically induced electron spin currents in the Kretschmann configuration, *Phys. Rev. B* **102**, 125431 (2020).
- [44] M. S. Ukhtary and R. Saito, Surface plasmons in graphene and carbon nanotubes, *Carbon* **167**, 455 (2020).
- [45] M. S. Ukhtary, Y. Tian, and R. Saito, Spin current generation by edge plasmons in graphene ribbons, *Phys. Rev. B* **103**, 245428 (2021).
- [46] Y. Tian, M. S. Ukhtary, and R. Saito, Switching performance of optically generated spin current at the graphene edge, *Phys. Rev. B* **106**, 045420 (2022).
- [47] A. Bekshaev, Spin-accumulation and spin-transport effects induced by surface plasmon-polariton waves, *J. Opt. Soc. Am. B* **39**, 3187 (2022).
- [48] C. Triolo, A. Cacciola, S. Patane, R. Saija, S. Savasta, and F. Nori, Spin-momentum locking in the near field of metal nanoparticles, *ACS Photon.* **4**, 2242 (2017).
- [49] P. Shi, L. Du, C. Li, A. Zayats, V. and X. Yuan, Transverse spin dynamics in structured electromagnetic guided waves, *Proc. Natl. Acad. Sci. (USA)* **118**, e2018816118 (2021).
- [50] N. Ichiji, D. Oue, M. Yessenov, K. L. Schepler, A. F. Abouraddy, and A. Kubo, Transverse spin angular momentum of a space-time surface plasmon polariton wave packet, *Phys. Rev. A* **107**, 063517 (2023).
- [51] A. Porfirev, S. Khonina, and A. Kuchmizhak, Light-matter interaction empowered by orbital angular momentum: Control of matter at the micro- and nanoscale, *Prog. Quantum Electron.* **88**, 100459 (2023).
- [52] J. Ni, S. Ji, Z. Wang, S. Liu, Y. Hu, Y. Chen, J. Li, X. Li, J. Chu, D. Wu, and C.-W. Qiu, Unidirectional unpolarized luminescence emission via vortex excitation, *Nat. Photon.* **17**, 601 (2023).
- [53] J. R. Rouxel, B. Roesner, D. Karpov, C. Bacellar, G. F. Mancini, F. Zinna, D. Kinschel, O. Cannelli, M. Oppermann, C. Svetina, A. Diaz, J. Lacour, C. David, and M. Chergui, Hard x-ray helical dichroism of disordered molecular media, *Nat. Photon.* **16**, 570 (2022).
- [54] A. Jain, J.-L. Begin, P. Corkum, E. Karimi, T. Brabec, and R. Bhardwaj, Intrinsic dichroism in amorphous and crystalline solids with helical light, *Nat. Commun.* **15**, 1350 (2024).
- [55] Y. Cao, S. Liu, Y. Tao, X. Wang, J. Ni, C. Wang, X. Zheng, J. Li, Y. Hu, D. Wu, and J. Chu, Photonic orbital angular momentum dichroism on three-dimensional chiral oligomers, *ACS Photon.* **10**, 1873 (2023).
- [56] N. Ichiji, T. Ishida, I. Morichika, T. Tatsuma, and S. Ashihara, Rotationally displaced electric field intensity distribution around square nanoantennas induced by circularly polarized light, *Phys. Rev. B* **109**, 035428 (2024).
- [57] M. Schäferling, D. Dregely, M. Hentschel, and H. Giessen, Tailoring enhanced optical chirality: Design principles for chiral plasmonic nanostructures, *Phys. Rev. X* **2**, 031010 (2012).
- [58] F. P. Schmidt, H. Ditlbacher, F. Hofer, J. R. Krenn, and U. Hohenester, Morphing a plasmonic nanodisk into a nanotriangle, *Nano Lett.* **14**, 4810 (2014).
- [59] M. Pellarin, J. Ramade, J. M. Rye, C. Bonnet, M. Broyer, M.-A. Lebeault, J. Lermé, S. Marguet, J. R. G. Navarro, and E. Cottancin, Fano transparency in rounded nanocube dimers induced by gap plasmon coupling, *ACS Nano* **10**, 11266 (2016).
- [60] G. Boudarham and M. Kociak, Modal decompositions of the local electromagnetic density of states and spatially resolved electron energy loss probability in terms of geometric modes, *Phys. Rev. B* **85**, 245447 (2012).